Concentration and relaxation rate independent clinical pH-weighted metabolic imaging at 3T using pulsed radiofrequency chemical exchange saturation transfer spin-and-gradient-echo echoplanar imaging (CEST-SAGE-EPI)

Jingwen Yao and Benjamin M. Ellingson

UCLA Brain Tumor Imaging Laboratory, Center for Computer Vision and Imaging Biomarkers

Department of Radiological Sciences, University of California Los Angeles

Introduction: Decrease in tissue pH is associated with many diseases including ischemic stroke, cancer, and seizure disorders[1]. Noninvasive pH measurement with chemical exchange saturation transfer (CEST) MRI can be challenging due to a variety of confounding factors. In this study, we investigate the feasibility of using a "ratiometric method" to obtain tissue relaxation rates and concentration independent pH-weighted MR image contrast at clinical field strengths using short RF saturation pulse trains and a multi-echo echoplanar readout.

Methods: *Theory:* A new metric $R(\Delta\omega_1, \Delta\omega_2)$ was calculated as the ratio of two inverse Z values[2] (Z is the normalized magnetization) at two different offset frequencies $\Delta\omega_1$ and $\Delta\omega_2$, normalized with respect to a reference frequency $\Delta\omega_{ref}$:

$$R(\Delta\omega_1, \Delta\omega_2) = \frac{Z(\Delta\omega_2)\left(Z\left(\Delta\omega_{ref}\right) - Z(\Delta\omega_1)\right)}{Z(\Delta\omega_1)\left(Z\left(\Delta\omega_{ref}\right) - Z(\Delta\omega_2)\right)}$$

The dependency of $R(\Delta\omega_1, \Delta\omega_2)$ on factors other than pH are mitigated by: (1) normalization of the inverse Z value with respect to a reference frequency to reduce the dependency on transverse water relaxation T_{2w} and macromolecule magnetization transfer (MT) effects; (2) use of short and high amplitude saturation pulses to ensure much stronger saturation effects on fast exchanging amine protons and lower effects on slower exchanging proton groups (**Figure 1(A)(B)**); (3) cancellation of longitudinal water relaxation T_{1w} and concentration effects through calculation of a ratio of inverse Z values. *Simulation:* Numerical simulation was performed on a four-pool chemical exchange system with bulk water pool, macromolecular bound water pool, amine proton pool, and amide proton pool. Ratiometric CEST values were calculated from the simulated spectra. The dependencies of $R(\Delta\omega_1, \Delta\omega_2)$ on water relaxation rates, amine and amide proton pool sizes, MT effect and saturation pulse amplitudes were subsequently investigated. *Phantom experiments:* Phantoms with different glutamine (amine) and protein (amide) concentrations were prepared with varying pH. A CEST echoplanar (EPI) sequence with multiple spin-and-gradient echo (SAGE) readouts (**Figure 1(C)**) was applied using three 100ms Gaussian saturation pulses[4]. $R(\Delta\omega_1, \Delta\omega_2)$ values were calculated with different MRI acquisition parameters (B_1=3μT/6μT), different choice of offset frequencies: $\Delta\omega_1/\Delta\omega_2$ = 3.0ppm/3.5ppm, 3.0ppm/3.8ppm, and mean(2.8-3.0ppm)/mean(3.8-4.0ppm) and different reference frequencies (6.0ppm or 20.0ppm), to evaluate the sensitivity and signal-to-noise ratio, and to find the optimum metric formulation. *In vivo imaging:* One healthy volunteer and one glioma patient

were scanned with the same sequence and parameters as the phantom experiments. The pH maps were calculated from the phantom $R(\Delta\omega_1, \Delta\omega_2)$-pH calibration.

Results: Results from numerical simulation and phantom experiments indicate that $R(\Delta\omega_1, \Delta\omega_2)$ has an approximately linear relationship with pH. The $R(\Delta\omega_1, \Delta\omega_2)$-pH relationship has little dependency on T_{1w}, amine and amide concentration, and macromolecular MT effect (**Figure 2 and 3**). However, change in T_{2w} noticeably alters $R(\Delta\omega_1, \Delta\omega_2)$-pH relationship (**Figure 3(B)**) due to the incomplete cancellation of T_{2w} effect at high saturation pulse amplitude. This potential limitation can be mitigated through estimates of T_2 using multi-echo readout and T_{2w}-correction with a simple bilinear fitting of $R(\Delta\omega_1, \Delta\omega_2)$ against pH and T_{2w} **(Figure 4)**. From the phantom experiment results, the ratio of the $R(\Delta\omega_1, \Delta\omega_2)$-pH slope and the mean standard deviation of $R(\Delta\omega_1, \Delta\omega_2)$ within regions of interest (ROIs) was calculated to assess the quantitative resolution of pH measurement (**Table 1**). The optimum sensitivity of pH measurement is found under the experimental condition of B_1=3μT, with $\Delta\omega_1/\Delta\omega_2$ = mean(2.8-3.0ppm)/mean(3.8-4.0ppm) and reference frequency at 6.0ppm, resulting in a $R(\Delta\omega_1, \Delta\omega_2)$-pH slope of -0.561. The optimum resolution of pH measurement is found with B_1=6μT, with the same $\Delta\omega_1/\Delta\omega_2$ and frequency of interest, resulting in a quantitative resolution of 0.13 pH units. Example *in vivo* MTRasym maps and pH maps are shown in **Figure 4(B)**.

Discussion: Compared to existing CEST-based pH quantification methods, the metric $R(\Delta\omega_1, \Delta\omega_2)$ has several advantages: (1) the short saturation pulse in combination with EPI readout makes it possible to acquire whole brain coverage high resolution pH-weighted CEST images in a clinically allowable scan time; (2) using only the positive Z-spectra points for $R(\Delta\omega_1, \Delta\omega_2)$ calculation avoids the contamination from nuclear Overhauser effects (NOE), which can complicate contrast based on asymmetry analyses (e.g. MTR_{asym}); (3) $R(\Delta\omega_1, \Delta\omega_2)$ does not require *a priori* knowledge of water relaxation rates, since the metric is independent of T_{1w} and T_{2w} correction can be achieved using a multi-echo SAGE EPI readout; (4) little dependency on amine and amide concentration; and (5) straightforward post-processing. Additionally, the approximate linear relationship between $R(\Delta\omega_1, \Delta\omega_2)$ and pH allows for quantitative pH estimation to be performed after initial calibration (e.g. ^{31}P-MRS).

Conclusion: This study proposed a new metric $R(\Delta\omega_1, \Delta\omega_2)$ as a noninvasive and easy-to-translate pH imaging technique that is not sensitive to water relaxation rates or amino acid concentration. This approach will be highly valuable for investigating metabolic changes in patients with a variety of diseases.

References:

[1] Chesler M. Regulation and modulation of pH in the brain. Physiol Rev 2003;83(4):1183-221.

[2] Zaiss M, Xu J, Goerke S, Khan IS, Singer RJ, Gore JC, et al. Inverse Z-spectrum analysis for spillover-, MT-, and T1-corrected steady-state pulsed CEST-MRI-application to pH-weighted MRI of acute stroke. NMR in biomedicine 2014;27(3):240-52.

[3] Zaiss M, Bachert P. Exchange-dependent relaxation in the rotating frame for slow and intermediate exchange-modeling off-resonant spin-lock and chemical exchange saturation transfer. NMR in Biomedicine 2013;26(5):507-18.

[4] Harris RJ, Cloughesy TF, Liau LM, Nghiemphu PL, Lai A, Pope WB, et al. Simulation, phantom validation, and clinical evaluation of fast pH-weighted molecular imaging using amine chemical exchange saturation transfer echo planar imaging (CEST-EPI) in glioma at 3 T. NMR in Biomedicine 2016;29(11):1563-76.

	Slope	Std.Dev.	-Slope/Std.Dev.
B_1 = 6μT reference 6.0ppm			
3.0ppm/3.5ppm	-0.064	0.052	1.234
3.0ppm/3.8ppm	-0.187	0.078	2.402
3.0ppm/4.0ppm	-0.249	0.102	2.435
mean(2.8-3.0ppm)/mean(3.8-4.0ppm)	-0.224	0.066	3.409
B_1 = 6μT reference 20.0ppm			
3.0ppm/3.5ppm	-0.080	0.032	2.541
3.0ppm/3.8ppm	-0.178	0.040	4.475
3.0ppm/4.0ppm	-0.228	0.046	4.913
mean(2.8-3.0ppm)/mean(3.8-4.0ppm)	-0.220	0.028	7.747*
B_1 = 3μT reference 6.0ppm			
3.0ppm/3.5ppm	-0.202	0.090	2.250
3.0ppm/3.8ppm	-0.412	0.130	3.172
3.0ppm/4.0ppm	-0.547	0.178	3.068
mean(2.8-3.0ppm)/mean(3.8-4.0ppm)	-0.561	0.108	5.200**
B_1 = 3μT reference 20.0ppm			
3.0ppm/3.5ppm	-0.155	0.058	2.700
3.0ppm/3.8ppm	-0.278	0.073	3.828
3.0ppm/4.0ppm	-0.340	0.089	3.826
mean(2.8-3.0ppm)/mean(3.8-4.0ppm)	-0.363	0.055	6.606

Table 1. Phantom $R(\Delta\omega_1, \Delta\omega_2)$-pH slope and $R(\Delta\omega_1, \Delta\omega_2)$ standard deviation. *: The optimum -Slope/Std.Dev was found with experimental condition of B_1 = 6μT, reference frequency at 20.0ppm and offset frequencies of interest at 2.8-3.0ppm and 3.8-4.0ppm. **: The optimum slope was found with experimental condition of B_1 = 3μT, reference frequency at 6.0ppm and offset frequencies of interest at 2.8-3.0ppm and 3.8-4.0ppm.

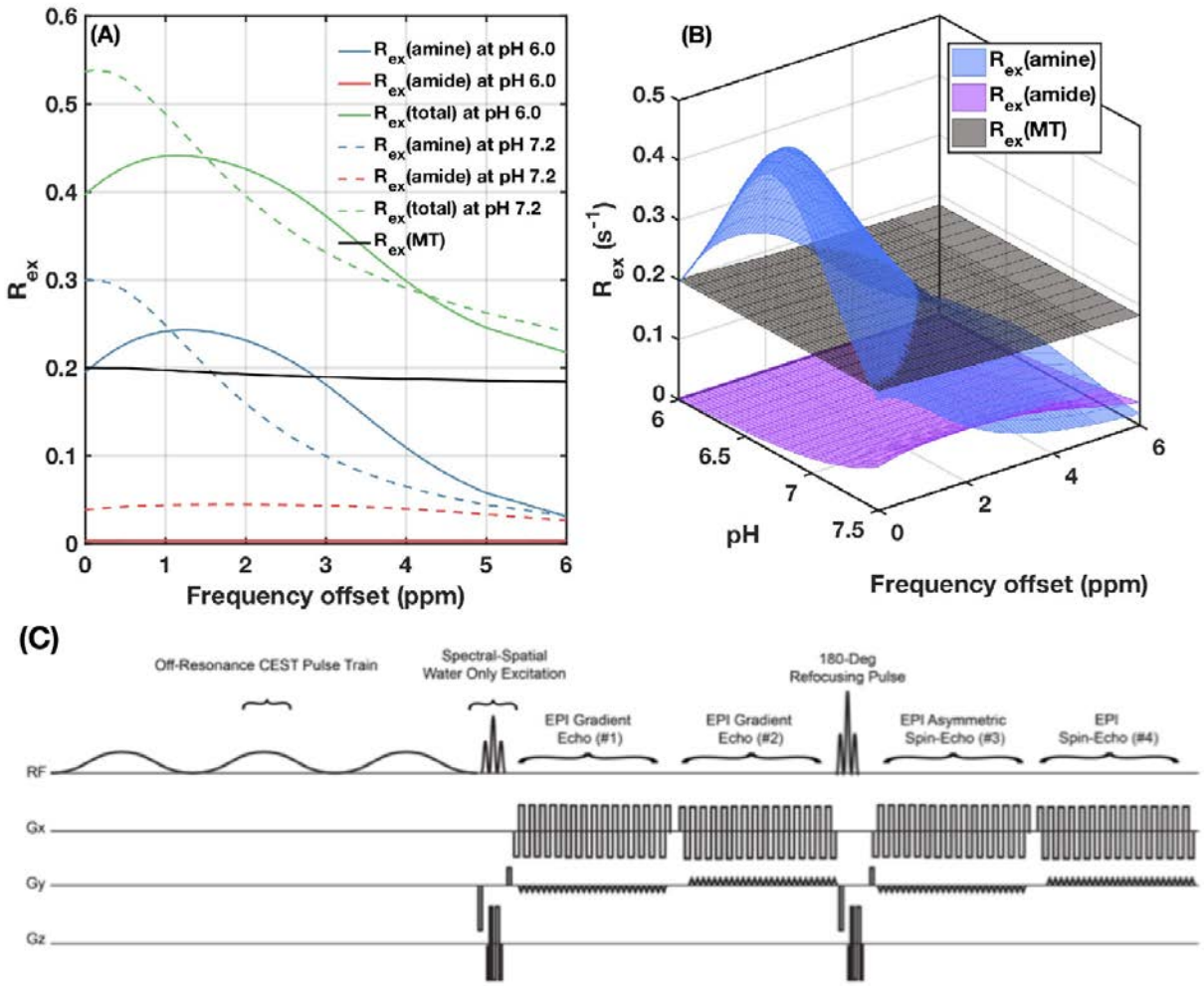

Figure 1. The pH and saturation frequency dependencies of R_{ex} (the exchange-dependent relaxation rate), and the pulse sequence diagram. (A) and (B) show the numerical values calculated from equation in the CEST model developed by Zaiss *et al.*[3], using B_1 amplitude of 6μT and assuming CEST contrast pool fraction f_{amine} = 0.00045, f_{amide} = 0.0013 and f_{MT} = 0.01. (C) shows the pulse sequence diagram for multi-echo CEST spin-and-gradient echo planar imag-ing (ME-CEST-SAGE-EPI).

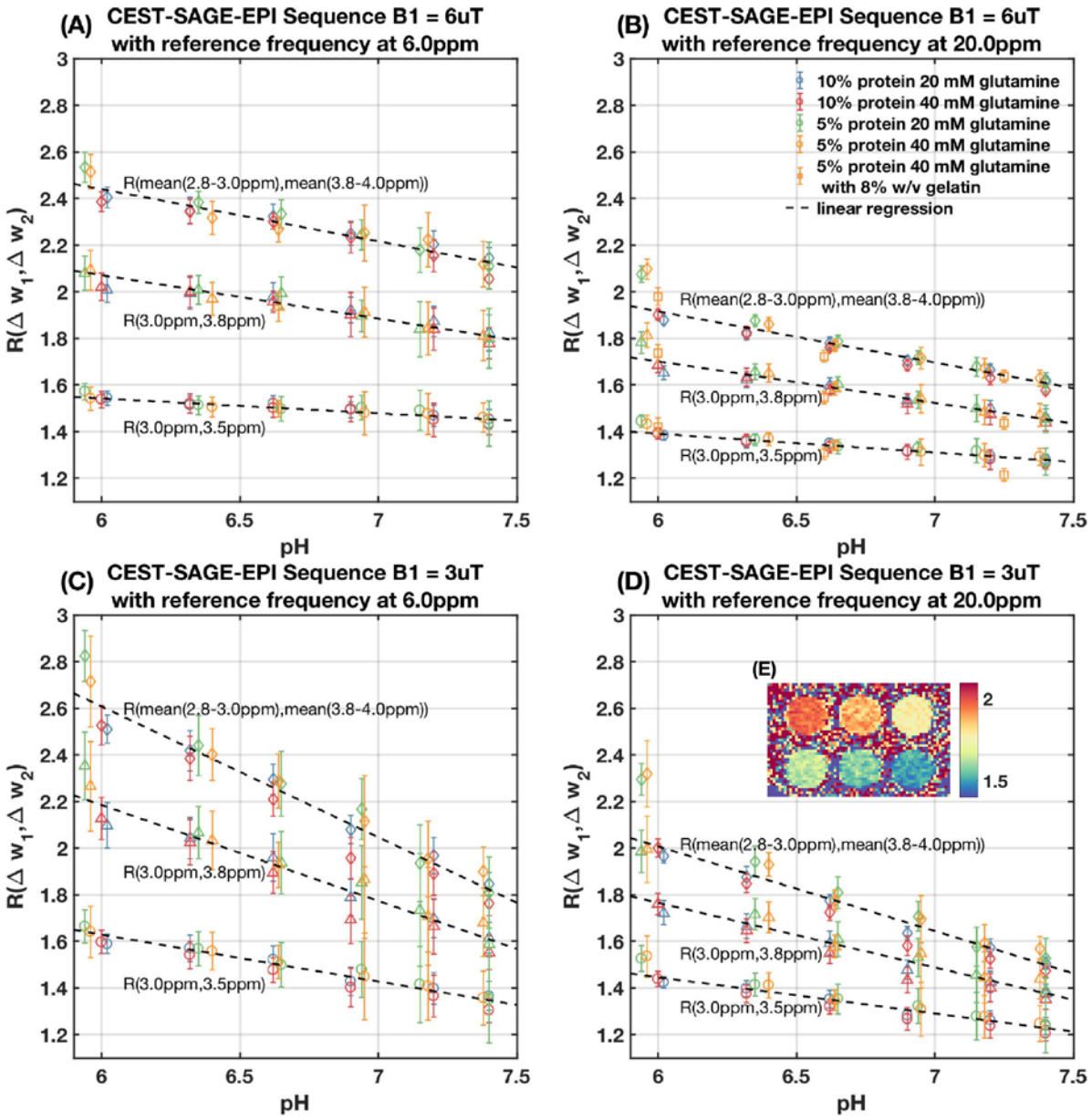

Figure 2. Phantom $R(\Delta\omega_1, \Delta\omega_2)$ dependencies on B_1 amplitude, reference frequency, offset frequency of interest, pH, amine concentration and protein concentration. The figure shows $R(\Delta\omega_1, \Delta\omega_2)$-pH relationship in four different experimental conditions: saturation amplitude B_1 = 6μT with reference frequency at 6.0ppm (A) or 20.0ppm (B); B_1 = 3μT with reference frequency at 6.0ppm (C) or 20.0ppm (D). In each subplot, data acquired from four different phantom compositions (see legend) with three different sets of $\Delta\omega_1$ and $\Delta\omega_2$ (3.0ppm/3.5ppm, 3.0ppm/3.8ppm, mean(2.8-3.0ppm)/mean(3.8-4.0ppm)) are plotted. Dashed lines represent the linear regressions of $R(\Delta\omega_1, \Delta\omega_2)$-pH relationship. (E) shows an example $R(\Delta\omega_1, \Delta\omega_2)$ map with (2.8-3.0ppm)/mean(3.8-4.0ppm).

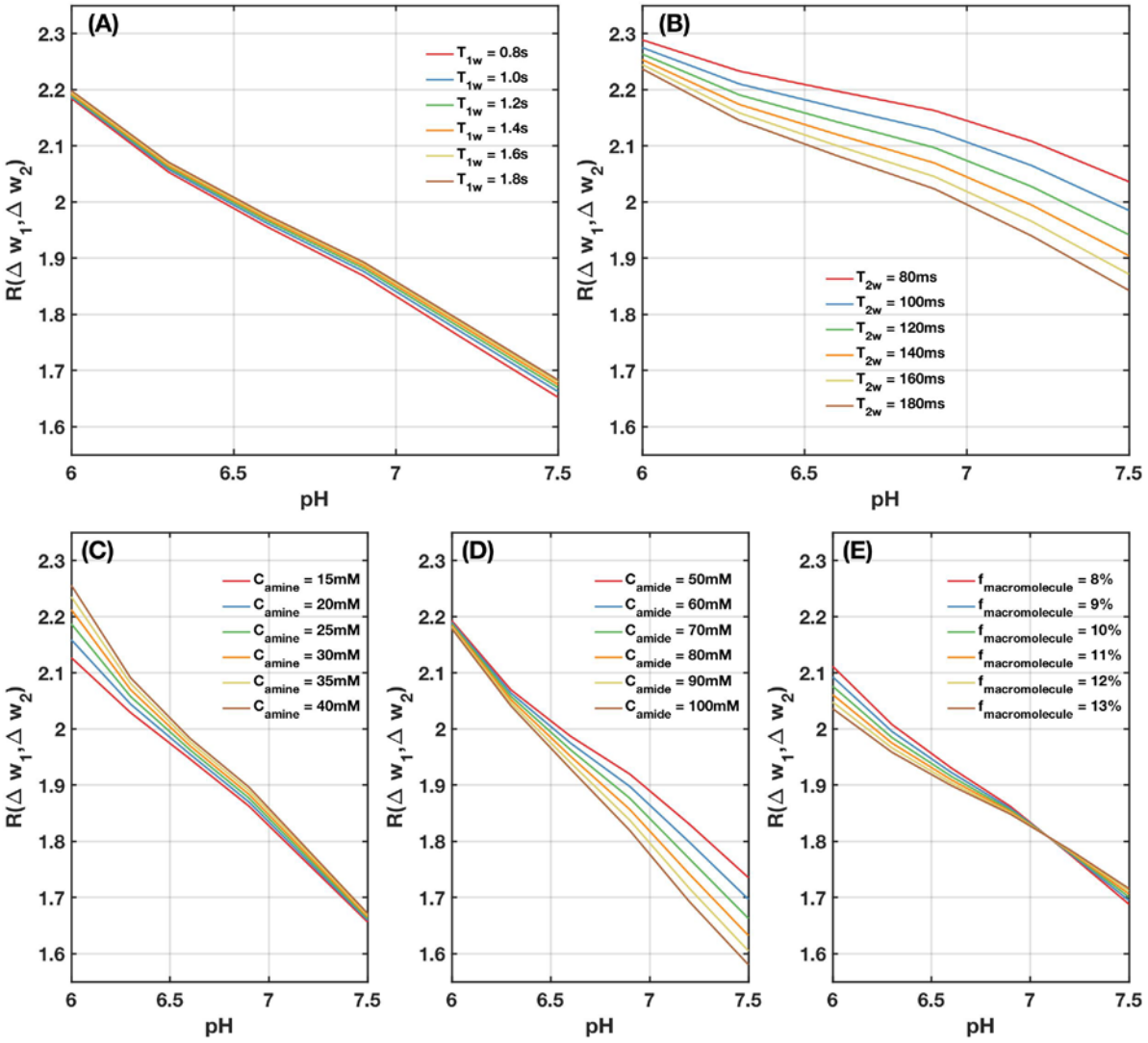

Figure 3. Simulated $R(\Delta\omega_1, \Delta\omega_2)$ values and the dependencies on pH, water relaxation rates, amine and amide concentrations, and macromolecular bound water pool size, with saturation pulse amplitude of B_1 = 3μT, reference frequency of 6.0ppm, and frequencies of interest of mean(2.8-3.0ppm) and mean(3.8-4.0ppm). (A) The dependency of $R(\Delta\omega_1, \Delta\omega_2)$ -pH relationship on T_{1w} (0.8s - 1.8s); (B) T_{2w} (80ms - 180ms); (C) amine concentration (15mM - 40mM); (D) amide concentration (50mM - 100mM); and (E) macromolecular concentration (8% - 13%). The $R(\Delta\omega_1, \Delta\omega_2)$-pH relationship shows no dependency on T_{1w}, some dependency on T_{2w}, and little dependency on CEST pool fractions.

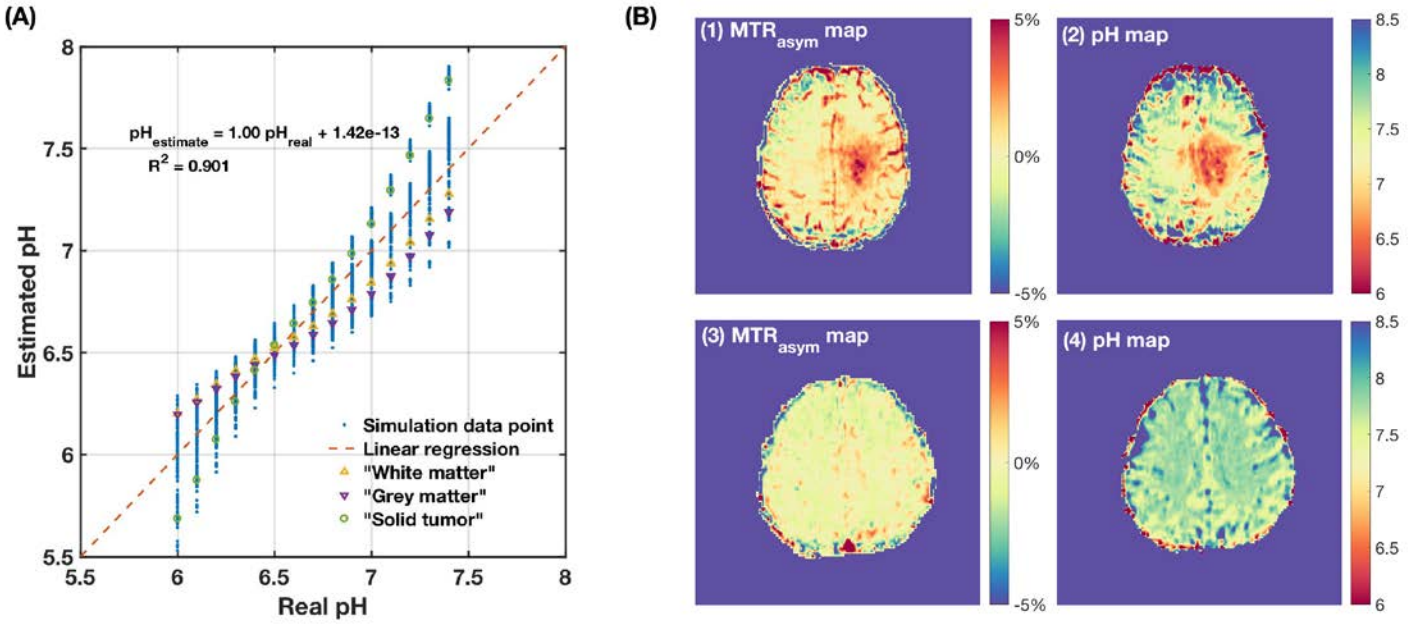

Figure 4. pH estimation calculated from T_{2w} corrected $R(\Delta\omega_1, \Delta\omega_2)$ and in vivo MRI images. (A) Data points represent the simulated pH estimations of tissue types with combinations of different T_{2w}, C_{amine}, and C_{amide} values, calculated from T_{2w} corrected $R(\Delta\omega_1, \Delta\omega_2)$. The three series of data points highlighted correspond to simulation parameters for white matter (T_{2w}=80ms, C_{amine}=15mM and C_{amide}=70mM), grey matter (T_{2w}=120ms, C_{amine}=10mM and C_{amide}=50mM) and solid tumor (T_{2w}=140ms, C_{amine}=40mM and C_{amide}=100mM). The estimated pH values highly correlate with real pH values, with little discrepancy. Figure (B) shows example MTR_{asym} maps and pH maps for glioma patient (1,2) and healthy volunteer (3,4).